Icy wave-cloud lunar corona and cirrus iridescence

Joseph A. Shaw* and Nathan J. Pust

Electrical and Computer Engineering Department, Montana State University, 610 Cobleigh Hall, Bozeman, Montana 59717, USA

*Corresponding author: jshaw@montana.edu

Received 29 June 2011; accepted 12 July 2011;
posted 22 July 2011 (Doc. ID 149923); published 12 August 2011

Dual-polarization lidar data and radiosonde data are used to determine that iridescence in cirrus and a lunar corona in a thin wave cloud were caused by tiny ice crystals, not droplets of liquid water. The size of the corona diffraction rings recorded in photographs is used to estimate the mean diameter of the diffracting particles to be 14.6 μm, much smaller than conventional ice crystals. The iridescent cloud was located at the tropopause [~11–13.6 km above mean sea level (ASL)] with temperature near −70 °C, while the more optically pure corona was located at approximately 9.5 km ASL with temperature nearing −60 °C. Lidar cross-polarization ratios of 0.5 and 0.4 confirm that ice formed both the iridescence and the corona, respectively.

OCIS codes: 010.1290, 010.2940, 010.3640, 290.1090, 290.5855, 280.4788.

1. Introduction

The colored swirls of iridescence and colored rings of the optical corona generally are explained as arising from diffraction of sunlight or moonlight by spherical water droplets in clouds [1–3]. For colors to be discernible by eye around the Sun or Moon requires the diffracting particles to have radius of the order of 10 μm, generally much smaller than ice crystals found in clouds. However, during the past two decades, several studies have documented the existence of corona and iridescence in ice clouds. For example, polarization lidar data and photographs were used to demonstrate ten cases of ice-cloud corona in northern Utah [4]. This methodology was later supplemented with *in situ* aircraft samples to show that a corona-producing thin cirrus cloud in northern Oklahoma contained 25 μm diameter ice crystals of unusual shape [5]. A similar study showed that ice-laden cirrus clouds also can create iridescence, which is a randomized diffraction pattern that arises when the spatial distribution of particle sizes is more random than for the corona (but still locally quite monodisperse) [6]. The conditions for ice-cloud coronas in all of these studies were thin cirrus clouds that were unusually high and cold for the middle latitudes [at or near the tropopause, typically ~11–13 km above mean sea level (ASL) with temperatures of −60 to −70 °C]. All cases generated large lidar cross-polarization ratios (typically 0.5–0.7). An explanation was proposed that the 25 μm ice crystals of somewhat unusual shape are formed when liquid droplets of sulfuric acid from the stratosphere freeze homogeneously as they become diluted during growth by water vapor rising up from the troposphere [5].

A related study was performed for mountain wave clouds [7,8], using photographs and meteorological analysis to show that coronas were generated in mountain wave clouds in northeastern Colorado under situations for which the clouds must have contained ice. That study did not benefit from either cloud particle samples or lidar data, but instead used previous *in situ* samples that showed that small quasi-spherical ice particles with diameters near 10–20 μm can exist in mountain wave clouds, presumably being unable to grow into more common sizes and shapes because of the high vertical velocities

0003-6935/11/2800F6-06$15.00/0

found in these unique clouds. However, because of the lack of measurements of the actual wave clouds forming those photographed coronas, there was still a need for more complete documentation of coronas in ice-containing wave clouds. This paper fills that gap by reporting dual-polarization lidar measurements of ice in a wave cloud while it was producing a visible lunar corona. This particular corona developed in a wave cloud that was observed after iridescence had been observed on and off for two days in a thicker cirrus. The atmospheric thermodynamic conditions measured with radiosondes show that both clouds contained ice, not liquid. The corona is documented in digital photographs that are analyzed using Fraunhofer diffraction theory to determine the effective size of diffracting ice particles. The conditions found for this cirrus iridescence are nearly identical to those reported previously for corona-producing cirrus and iridescence [4–6], but the ice wave-cloud corona was located at a slightly lower altitude and warmer temperature.

2. Observations and Measurements

A. Cirrus Iridescence

On the afternoon of 3 February 2009 in Bozeman, Montana (45.67 °N, 111.05 °W), iridescence became visible in a high-altitude cirrus cloud, which was found with a combination of lidar and radiosonde data to be located at the height of the tropopause, 13.5 km ASL. Figure 1 is a photograph of this iridescence display taken at 1600 Mountain Standard Time (MST = UTC – 7), showing a typical variety of pastel reds, greens, and blues. The significant amount of green present in this display may suggest that this particular cloud does not have quite the low optical depth and narrow particle-size distribution that simulations show are required to produce blue as the dominant short-wavelength color [3,8]. However, the colors observed in iridescence displays also can change significantly with the angle of illumination. This display of iridescence remained visible during periods when the Sun and clouds were favorably located in the sky throughout 3–4 February. The atmospheric thermodynamic conditions during this time are discussed in Subsection 2.D.

Fig. 1. (Color online) Photograph of iridescence in cirrus cloud (altitude = 13.4 km ASL) on 3 February 2009 at 1600 MST (2300 UTC). Photo by J. A. Shaw using a Nikon D300 and an 18–200 mm VR zoom lens set at 60 mm, ISO250, $f/14$, 1/800 s exposure.

B. Wave-Cloud Corona

On the evening of 5 February 2009, beginning about 1900 MST (6 February, 0200 UTC), a colorful lunar corona was observed in a thin wave cloud fortuitously located near the zenith in Bozeman, Montana. Stars were visible through the cloud and at least two orders of diffraction rings could be distinguished in the corona. A photograph of this corona alongside a green laser beam from the Montana State University dual-polarization lidar is shown in Fig. 2. The photograph sufficiently exposes the second-order red ring on the outside, the second-order blue ring in the middle, and the first-order red ring on the inside. The first-order blue ring is lost in the overexposed center region containing the waxing Moon, which was full on 9 February. Coronas with multiple visible diffraction orders are fairly common in wave clouds because of the tendency of these clouds toward monodisperse

Fig. 2. (Color online) Photograph of lidar beam and lunar corona on 4 February 2009 at 2032 MST (6 February, 0332 UTC). Photograph by J. A. Shaw using a Nikon D300 camera, a 10.5 mm fisheye lens, ISO 400, $f/2.8$, 4.0 s exposure.

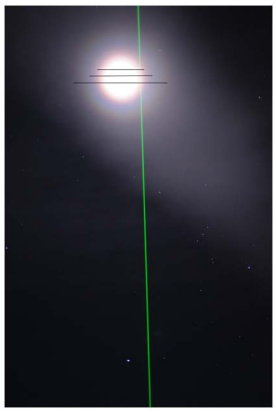

Fig. 3. (Color online) Lunar corona photograph used for the diffraction analysis [photograph by J. A. Shaw on 4 February 2009 at 2034 MST (6 February, 0332 UTC), using a Nikon D300 camera and a 20 mm fisheye lens, ISO 1000, $f/2.8$, 2.0 s exposure]. The three horizontal black lines across the corona indicate the diameters of the first-order red ring (top), the second-order blue ring (center), and the second-order red ring (bottom).

particle-size distributions with relatively small mean particle sizes [7,8].

C. Diffraction Analysis of Corona Photographs

Fraunhofer diffraction theory allows estimation of the size of the cloud particles from the angular extent of the corona rings [1,7,8]. For circular objects of diameter D, the diffraction pattern contains concentric colored rings with maxima located such that

$$\frac{Dr}{\lambda z} \approx \frac{D\theta_r}{\lambda} = 0, 1.635, 2.679, 3.699\ldots, \quad (1)$$

and minima located such that

$$\frac{Dr}{\lambda z} \approx \frac{D\theta_r}{\lambda} = 1.220, 2.233, 3.238\ldots, \quad (2)$$

where r is the radial coordinate in the observation plane, z is the distance from the diffracting object to the observation plane, θ_r is the angular radius of the diffraction ring, and λ is the optical wavelength [9]. A similar set of equations with maxima and minima located at integer values would apply if we treated this as randomly oriented particles of rectangular cross section (instead of circular) [9]. However, the difference this would make falls within the uncertainties that arise from picking an appropriate monochromatic wavelength or locating the exact location of the corona minima or maxima. Here we use Eq. (1) to solve for D using θ_r measured from a digital photograph of the corona for a wavelength λ chosen to match the color of a particular ring.

Table 1. Corona Ring Dimensions and Resulting Cloud Particle Diameter

Ring Description	N_{dia} (pixels)	Angular Radius (mrad)	Cloud Particle Dia. (μm)
First-order red max.	483	63.8	16.2
Second-order red max.	984	129.9	13.0
Second-order blue max.	691	91.2	14.5
			Mean = 14.6 μm

Instead of the wide-angle image of Fig. 2, the diffraction analysis was performed on the narrower-field-of-view image shown in Fig. 3 (the horizontal black lines across the corona indicate, from top to bottom, the diameters of the first-order red ring, the second-order blue ring, and the second-order red ring). This image was recorded with a Nikon D300 camera through a lens with focal length $f = 20$ mm. The camera's sensor has dimensions of 23.6 mm× 15.8 mm, so the short-axis angular width of the image is found as twice the half-field-of-view angle:

$$\alpha_{\text{image}} = 2\tan^{-1}\left(\frac{15.8}{2f}\right). \quad (3)$$

With a focal length of 20 mm, this results in an angular width of 752.4 mrad (43.1°) for the image of Fig. 3. The sensor contains 4288 × 2848 pixels, so the short-axis angular pixel resolution is

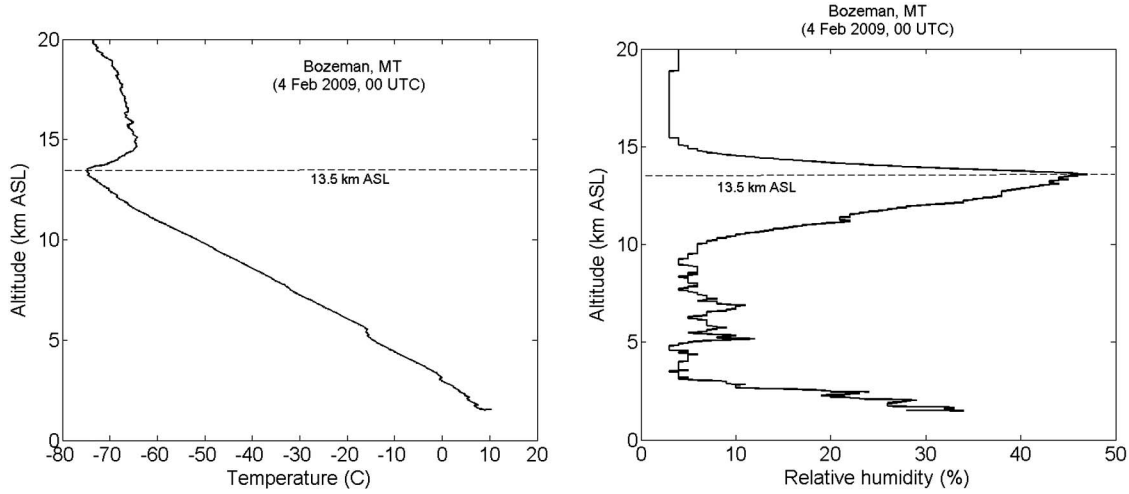

Fig. 4. Radiosonde profiles of atmospheric temperature (left) and relative humidity (right) above Bozeman, Montana (ground altitude ~1.5 km) near 1700 MDT on 3 February 2009 (0000 UTC on 4 February) during the iridescence display of Fig. 1.

Table 2. Tropopause Altitudes and Temperatures from Synoptic Soundings at Great Falls, Montana

Time (UTC)	Date	Tropopause Altitude (km ASL)	Tropopause Temperature (°C)
0000	3 Feb.	13.0	−76
1200	3 Feb.	13.0	−79
0000	4 Feb.	13.6	−79
1200	4 Feb.	13.0	−75
0000	5 Feb.	12.7	−78
1200	5 Feb.	12.6	−70
0000	6 Feb.	11.7	−67
1200	6 Feb.	10.0	−61
0000	7 Feb.	9.4	−59
1200	7 Feb.	10.2	−58

$$\Delta\theta_{\text{pixel}} = \frac{\alpha_{\text{image}}}{\#\text{pixels}} = \frac{752.4\,\text{mrad}}{2848\,\text{pixels}} = 0.264\,\text{mrad/pixel}. \tag{4}$$

The angular diameter of the corona ring is found by multiplying N_{dia}, the number of pixels within the ring diameter, by the angular pixel resolution of Eq. (4). Then, to obtain the angular radius required for Eqs. (1) and (2), we divide the angular diameter in half to obtain the angular radius of the diffraction ring, θ_r:

$$\theta_r = \frac{N_{\text{dia}}\Delta\theta_{\text{pixel}}}{2}. \tag{5}$$

The angular radii found from Eqs. (4) and (5) for the first-order red, second-order red, and first-order blue corona rings are listed in Table 1, along with the corresponding mean cloud particle diameter values that result from solving Eq. (1) for D using the results of Eq. (5) for assumed wavelengths of 630 nm for the red rings and 490 nm for the blue ring. The results are reasonably repeatable, with the mean cloud particle diameter being estimated as $14.6 \pm 1.6\,\mu$m. The primary uncertainties are in locating the diffraction pattern maxima and estimating the appropriate wavelength for each ring (the latter uncertainty could be reduced by photographing through a narrowband optical filter to isolate the corona ring of a specific wavelength, but even then the selection of a single wavelength for diffraction analysis also is influenced by the width of the actual particle-size distribution in the cloud). The cloud particle diameters resulting from this analysis are quite similar to the values found previously for corona-producing cirrus (12–30 μm [4] and 22 μm [5]) and corona-producing wave clouds (7.6–24.3 μm [7]). An essentially identical value of 14.4 μm is obtained for the mean cloud particle diameter if we use the value 2.736° for the angular width of Orion's belt (visible in Fig. 3 below the corona and to the right of the lidar beam) in place of Eq. (3) to determine the angular width of the image.

D. Atmospheric Thermodynamic Conditions

Shortly after iridescence became visible in cirrus on the afternoon of 3 February 2009, a radiosonde was launched from the roof of the engineering building at Montana State University—Bozeman to measure vertical profiles of atmospheric temperature and humidity. These profiles clearly show the existence of a cloud at approximately 13.5 km ASL (Fig. 4). Our dual-polarization lidar [10] also measured the cloud height to be 13.5 km ASL, with cross-polarization ratio reaching as high as 0.55.

Synoptic soundings from radiosondes launched by the U.S. National Weather Service at Great Falls, Montana (the nearest synoptic sounding site, located ~200 km N of Bozeman) show that the tropopause dropped from 13.6 km ASL in the 0000 UTC, 4 February sounding to 9.0 km ASL in the 1200 UTC, 7 February sounding and then rose again. The tropopause altitudes and temperatures from the Great Falls soundings during the period of 3–7 February are listed in Table 2. The iridescence was observed

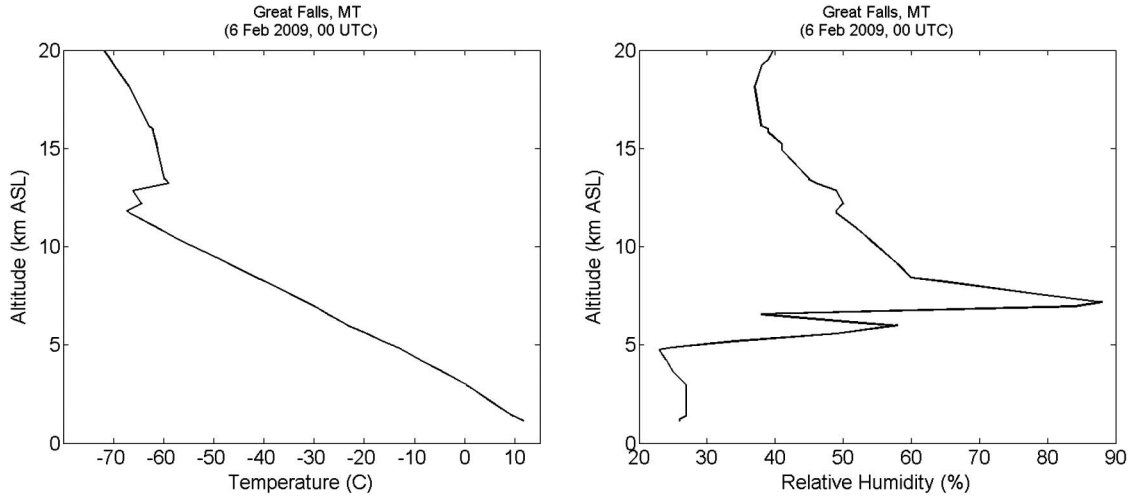

Fig. 5. Synoptic radiosonde profiles of temperature (left) and humidity (right) at 00 UTC, 6 February 2009, from Great Falls, Montana. The lunar corona observations (Fig. 2) were made during 0200-0400 UTC on 6 February 2009 while the tropopause was beginning to lower from 11.7 km at 00 UTC to 10.0 km at 12 UTC.

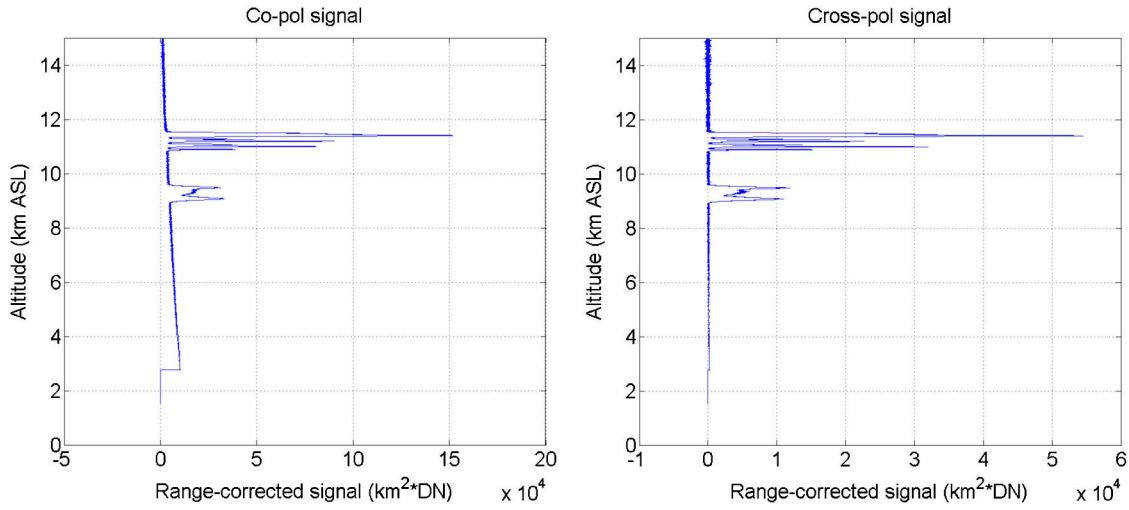

Fig. 6. (Color online) Altitude plot of range-corrected relative lidar backscatter signal at 0330 UTC on 6 February 2009: (left) copolarized signal and (right) cross-polarized signal.

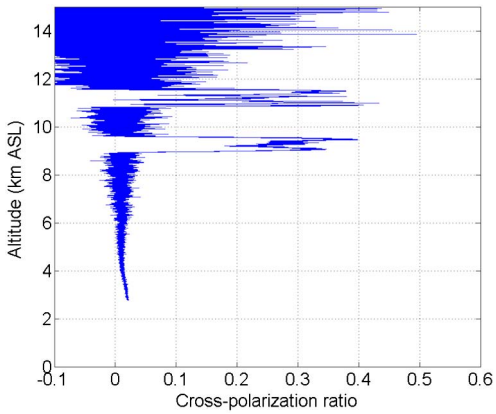

Fig. 7. (Color online) Altitude plot of lidar cross-polarization ratio at 0330 UTC, 6 February 2009, showing ice clouds at 9.5 and 11.3 km ASL (and zero-mean noise above the second cloud layer).

in cirrus clouds at or just below the tropopause during times corresponding to the 4–5 February soundings, and the corona was observed in a wave cloud located approximately 2 km below the tropopause 2–3 h after the 6 February 00 UTC sounding (Fig. 5). During the 2 h lunar corona observation period (5 February, 1900-2100 MST, or 6 February, 0200-0400 UTC) the near-surface air temperature remained 7 ± 1 °C and the near-surface relative humidity remained $30 \pm 2\%$.

E. Dual-Polarization Lidar Measurements

We collected laser backscatter data for 30 min during the peak of the lunar corona display (6 February, 0317-0347 UTC) using a dual-polarization lidar [10]. This instrument transmits a single linear polarization state at a wavelength of 532 nm and uses liquid crystal variable retarders to measure the backscattered laser signal in the transmitted linear polarization state and in an orthogonal linear polarization state on alternate laser pulses. Doing this with a pulse repetition frequency of 30 Hz allows measurement of the volume cross-polarization ratio (ratio of copolarized to cross-polarized signal, often called the "depolarization ratio" in the lidar community) for pairs of laser pulses at a frequency of 15 Hz. During this time, there were consistently two distinct, dissipating cloud layers: a thin cirrus layer at ~11.3 km ASL, and a wave cloud near the zenith sky at ~9.5 km ASL. The optical depth for the combined cloud layers faded from 0.75 to 0.06 during this time. The corona photographs of Figs. 2 and 3 were taken near the peak of the corona display, when the combined cloud optical depth was approximately 0.18. There were times during the observation period when the wave-cloud lidar return was greater than the cirrus return, but generally the wave-cloud return was smaller, as shown in the vertical profiles of range-corrected relative backscatter signal of Fig. 6. Throughout the lidar observation period, the cross-polarization ratio shown in Fig. 7 remained almost exactly 0.4 for each cloud layer.

3. Conclusion

Iridescence- and corona-producing ice clouds have been studied with a combination of diffraction analysis on digital photographs, radiosonde profiling of atmospheric thermodynamic conditions, and dual-polarization lidar measurements. The iridescence was a result of scattering of sunlight by tiny ice crystals in cirrus clouds located at the tropopause, with altitudes in the range of 12–13.6 km ASL and temperatures in the range of −70 to −79 °C. The corona was a result of scattering of moonlight by tiny ice crystals in a wave cloud located approximately 1.8 km below the tropopause at 9.5 km, with cloud temperature near −56 °C and tropopause temperature of approximately −70 °C. That both the cirrus and wave clouds were ice, not liquid, is confirmed by both the high lidar cross-polarization ratios of 0.55 and 0.40, respectively, and the extremely cold atmospheric temperatures, which were well below the temperature range where supercooled liquid can exist. Diffraction analysis applied to digital images of

the corona yielded a mean cloud particle diameter of $14.6 \pm 1.6\,\mu$m. This study provides independent confirmation of previously observed conditions that lead to iridescence (and corona) in cirrus, and provides the first known direct measurement of corona produced under similar conditions in a wave cloud.

This material is based on research sponsored by the Air Force Research Laboratory, under agreement number FA9550-10-1-0115.

References

1. J. A. Lock and L. Yang, "Mie theory of the corona," Appl. Opt. **30**, 3408–3414 (1991).
2. S. D. Gedzelman, "Simulating halos and coronas in their atmospheric environment," Appl. Opt. **47**, H157–H166 (2008).
3. S. D. Gedzelman and J. A. Lock, "Simulating coronas in color," Appl. Opt. **42**, 497–504 (2003).
4. K. Sassen, "Corona-producing cirrus cloud properties derived from polarization lidar and photographic analyses," Appl. Opt. **30**, 3421–3428 (1991).
5. K. Sassen, G. G. Mace, J. Hallett, and M. R. Poellot, "Corona-producing ice clouds: a case study of a cold mid-latitude cirrus layer," Appl. Opt. **37**, 1477–1485 (1998).
6. K. Sassen, "Cirrus cloud iridescence: a rare case study," Appl. Opt. **42**, 486–491 (2003).
7. J. A. Shaw and P. J. Neiman, "Coronas and iridescence in mountain wave clouds," Appl. Opt. **42**, 476–485 (2003).
8. P. J. Neiman and J. A. Shaw, "Coronas and iridescence in mountain wave clouds over northeastern Colorado," Bull. Am. Meteorol. Soc. **84**, 1373–1386 (2003).
9. J. W. Goodman, *Introduction to Fourier Optics* (McGraw-Hill, 1996).
10. N. L. Seldomridge, J. A. Shaw, and K. S. Repasky, "Dual-polarization lidar using a liquid crystal variable retarder," Opt. Eng. **45**, 106202, doi:10.1117/1.2358636 (2006).